Perspectives on empirical approaches for ocean color remote sensing of chlorophyll in a changing climate

Heidi M. Dierssen[1]
Department of Marine Sciences/Geography, University of Connecticut, Groton, CT 06340

Edited by David M. Karl, University of Hawaii, Honolulu, HI, and approved August 24, 2010 (received for review November 30, 2009)

Phytoplankton biomass and productivity have been continuously monitored from ocean color satellites for over a decade. Yet, the most widely used empirical approach for estimating chlorophyll *a* (Chl) from satellites can be in error by a factor of 5 or more. Such variability is due to differences in absorption and backscattering properties of phytoplankton and related concentrations of colored-dissolved organic matter (CDOM) and minerals. The empirical algorithms have built-in assumptions that follow the basic precept of biological oceanography —namely, oligotrophic regions with low phytoplankton biomass are populated with small phytoplankton, whereas more productive regions contain larger bloom-forming phytoplankton. With a changing world ocean, phytoplankton composition may shift in response to altered environmental forcing, and CDOM and mineral concentrations may become uncoupled from phytoplankton stocks, creating further uncertainty and error in the empirical approaches. Hence, caution is warranted when using empirically derived Chl to infer climate-related changes in ocean biology. The Southern Ocean is already experiencing climatic shifts and shows substantial errors in satellite-derived Chl for different phytoplankton assemblages. Accurate global assessments of phytoplankton will require improved technology and modeling, enhanced field observations, and ongoing validation of our "eyes in space."

biological oceanography | phytoplankton | primary productivity | satellite oceanography | ocean optics

Since the Coastal Zone Color Scanner launched in 1978, chlorophyll *a* (Chl) has been derived from satellite measurements of ocean color and used to assess phytoplankton biomass, primary production, and the ocean's impact on the climate cycle (1, 2). The basic approach for remote sensing Chl follows from the premise that phytoplankton shift the reflected color spectrum from predominantly blue to green (3, 4). Standard calculation of Chl involves an empirical relationship developed from field observations of Chl and ocean color collected throughout the global ocean. Empirical approaches are used because an analytical solution to the problem requires an assessment of the entire radiance distribution and depth derivative (5), and such measurements are not possible with remote sensing. Only the upward flux incident upon the water/air interface at angles less than 48°, the angle at which complete internal reflection occurs, arrives above the sea surface, and generally only photons traveling roughly perpendicular to the sea surface are sensed from space (6). The current empirical algorithms have been applied to the vast majority of the ocean waters, historically termed "case 1" (4), where sea-surface optical properties vary primarily as a function of changes in phytoplankton biomass.

The apparent success of the empirical algorithm has led to the common misperception that ocean color remote sensing is a tractable problem that can be moved away from basic science and into the "operational" realm. Empirical algorithms, however, are only gross generalizations about phytoplankton biomass stemming primarily from implicit assumptions about how light is absorbed and scattered in surface waters. Many compelling climate-related changes in global phytoplankton biomass have been attributed to satellite-derived estimates of surface Chl, including a decline in productivity since 1999 (2) and the expansion of low-productivity regions (7, 8). However, temporal and spatial differences in ocean color may not be the result of changing Chl or phytoplankton biomass per se but from shifts in phytoplankton assemblages, physiology, or other optically active substances like colored-dissolved organic matter (CDOM). Furthermore, only surface waters are imaged with passive remote sensing and then correlated to depth-integrated phytoplankton biomass. Regions such as the Arctic, however, show a decoupling of surface and deep phytoplankton biomass that are not assessed with passive ocean-color measurements (9). Interpretations of any regional or climate-related trends in satellite-derived chlorophyll require a better understanding of the theoretical underpinnings of the empirical algorithms.

Oceanic carbon fixation must be quantified to assess the fate of atmospheric carbon dioxide and potential changes in climate. Phytoplankton photosynthesis promotes absorption of carbon dioxide from the atmosphere, and export of fixed carbon to the ocean interior provides a long-term sink for atmospheric carbon dioxide (10). Though satellite-derived Chl is not a direct measure of carbon fixation in phytoplankton, such estimates are typically derived from correlates of Chl and rates of carbon fixation (11). These relationships vary with phytoplankton species assemblages and their physiological state related to light, temperature, nutrients, and other environmental factors (12). Here, the most widely used and published empirical ocean color algorithm for Chl is explored with the hope that better interpretation of such data may also lead to improved estimates of primary productivity and the global carbon budget, particularly in a changing ocean. Large inputs of glacial meltwater, changes in stratification, ocean acidity, upwelling, and the magnitude and duration of storms may alter ocean life over the next century (13), (14). Such changes will influence the manner in which light is absorbed and scattered out of the world ocean and the approaches for determining Chl, carbon fixation, and other biogeochemical parameters from space.

Principles and Limitations of Empirical Algorithms

Empirical ocean color (OC) algorithms use two bands (OC2), three bands (OC3), or four bands (OC4) for global processing of imagery. The ocean color empirical algorithm, OC4V4, developed for the Sea-Viewing Wide Field-of-View Sensor (SeaWiFS), was derived from an optical dataset of the world's ocean spanning Chl concentrations from 0.02 to 50 $mg{\cdot}m^{-3}$ (15). The algorithm quantifies Chl as a function of the how much blue and green light is reflected from the sea surface. Numerically, a simple ratio of blue light (443, 490, or 510 nm, depending on which is greater) to green light (555 nm) is used. This basic "band ratio" approach has been carried forward to recent updates of

Author contributions: H.M.D. designed research, performed research, analyzed data, and wrote the paper.

The author declares no conflict of interest.

This article is a PNAS Direct Submission.

[1]E-mail: heidi.dierssen@uconn.edu.

the algorithm with only minor modifications to the empirical coefficients (e.g., OCv6).

The OC4V4 algorithm is a fourth-order polynomial fitting the average trend of the data (Fig. 1*A*). Superimposed lines show predicted OC4V4 Chl concentrations occurring within factors of 2–5 of the measured Chl. The global ocean is largely oligotrophic with a median Chl value around 0.2 mg·m^{-3} (Fig. 1*B*). Fortunately, the model performs best at low Chl (<0.2 mg Chl·m^{-3}) where values generally fall within a factor of 2 of model predictions. At high Chl, however, data are scattered within a factor of 5 of the modeled values, well outside the satellite data product accuracy goals of ±35% for Chl in the open ocean (16).

Particularly on a log-log plot, the human eye has a tendency to evaluate model performance based on the clustering of points near the trend line rather than the applicability of the model. The actual algorithm describes data following along a single reflectance ratio in the *x* axis, not the nearest data to the line. For example, if a sensor measured a blue-to-green reflectance ratio of 0.7, the data fitting that ratio, shown as the vertical magenta line in Fig. 1*A*, ranges from 1.7 to more than 30 mg·m^{-3}. The OC4V4 model would capture all of that variability as only one Chl value of 7.7 mg·m^{-3}.

The OC4V4 model has essentially three different slopes in the polynomial relationship: a gentle (−1.6), intermediate (−2.4), and a steep slope (−3.6), corresponding to increasing amounts of Chl in the water column (Fig. 1*A*). These changing slopes arise largely from switching between different wavelengths of light in the numerator of the model. For water containing low amounts of Chl (<0.7 mg·m^{-3}), mostly blue light leaves the water surface (Fig. 2*A*) and the shortest blue wavelength of light (443 nm) is used in the model. As Chl increases, more of the blue light is absorbed and the maximum wavelength of reflected light shifts toward the longer or "greener" wavelengths of light. The relationship becomes steepest at high Chl (>1 mg·m^{-3}), when 510 nm is used in the numerator. Empirical algorithms are selected based on a host of statistical parameters and graphical criteria (17), but no consideration is given to the steepness of the slope. Particularly on a log-log plot, a relationship with a steep slope will not be as robust to errors in sensor calibration, atmospheric correction, or other sources of noise in the satellite imagery and can lead to large errors in retrieved Chl.

This empirical model is not widely applicable to coastal waters because freshwater plumes with CDOM and minerals significantly impact the optical properties (18). Moreover, nutrient fertilization from terrestrial runoff can change phytoplankton dynamics and even produce harmful algal blooms that appear red in color (19). Melting and runoff of glacial sources can increase particle concentrations in the nearshore and change phytoplankton assemblages (20, 21). Under shifting environmental conditions, such localized phenomena may move beyond the coastal perimeter and require new approaches throughout the world ocean.

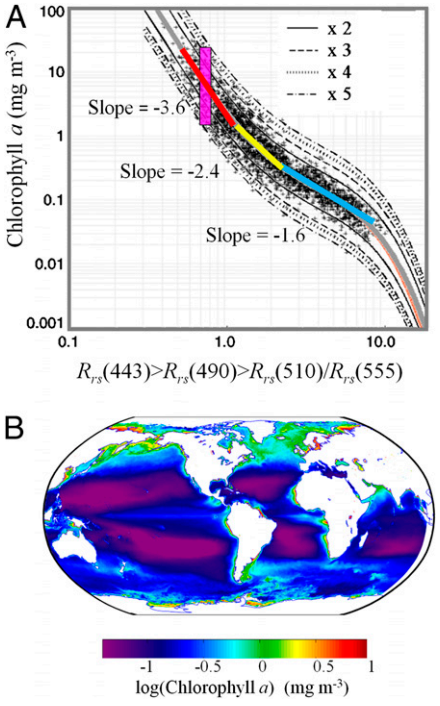

Fig. 1. (*A*) The empirical OC4V4 chlorophyll *a* algorithm used for the SeaWiFS sensor, which has produced the longest record of global Chl, shown with the original spectral reflectance (R_{rs}) data from which it was derived (17) and lines indicating data within two- to fivefold of the relationship. Different slopes in the model are due to the wavelength switching from the R_{rs}(443) at low Chl, R_{rs}(490) at middle Chl, and R_{rs}(510) at high Chl. The magenta bar illustrates the large variability in data when the relationship has the steepest slope. (*B*) Average composite SeaWiFS satellite-derived Chl from 1997 to 2009 for the world ocean.

Data Uncertainties

Some of the large variability in the empirical data (Fig. 1*A*) could result from errors in the radiometric and Chl measurements. Remote sensing reflectance, R_{rs}, is expressed as water-leaving radiance normalized to incident irradiance on the sea surface and is derived from other measurements. Measurements made above the sea surface must be corrected for surface-reflected light (i.e., light that has not penetrated the water column), and measurements made from within the water column must be extrapolated to a theoretical depth just beneath the sea surface (0^-) and then numerically extrapolated across the air-water interface (0^+). A recent analysis of R_{rs} measurements suggests that the largest errors occur in the Soret or blue band, with uncertainties on the order of 9% spectrally (22). When considering spectral band ratios, such as those used by the OC algorithms, uncertainties were reduced to 3%. Errors can be larger with less-well-calibrated instruments, different sampling protocols, and challenging environmental conditions (e.g., large capillary and gravity waves, sun glitter, etc.).

Measurements of Chl, however, are subject to potentially greater errors than the radiometric measurements. Historically, Chl has been derived from filtered fluorometric measurements following standard methods (23). Even standardized

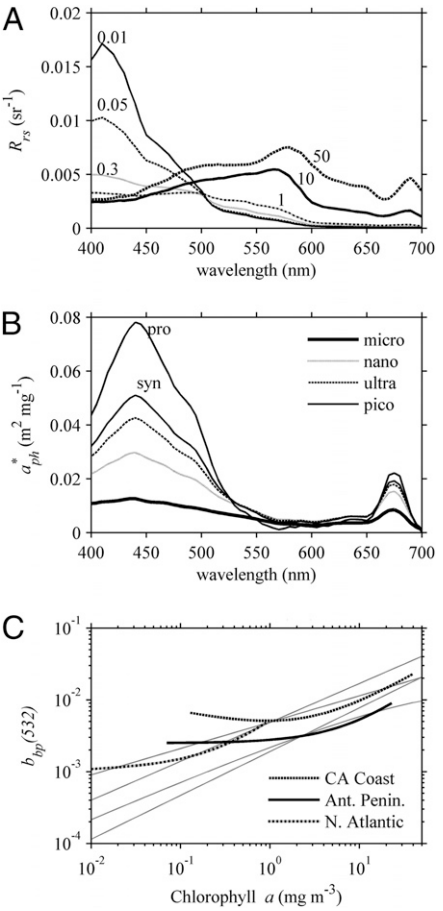

Fig. 2. (*A*) Example relationship of how remote sensing reflectance, R_{rs}, changes from blue peaked to green peaked with increasing chlorophyll. (*B*) The spectral shape and magnitude of chlorophyll-normalized absorption, a^*_{ph}, changes for different sizes of phytoplankton (30). (*C*) The bio-optical relationships between particulate backscattering and chlorophyll vary either linearly or log linearly, depending on the region. The straight lines represent several different bio-optical models (4, 37, 38).

methods, however, will yield different results depending on the composition of pigments within the phytoplankton, and errors can be on the order of 50% (24–26). The presence of significant amounts of chlorophyll *b*, characteristic of chlorophytes, prochlorophytes, and cryptophytes, causes fluorometric techniques to underestimate Chl. Conversely, high concentrations of chlorophyll *c*, typically found in diatoms, dinoflagellates, prasinophytes, and haptophytes, lead to an overestimation of Chl with respect to fluorometric measurements. Such pigment differences can be important for regions like the Southern Ocean. The several-fold variability shown in Fig. 1*A* is larger than these 3–50% measurement errors, however, and much of it can be explained by known variability in phytoplankton and CDOM properties.

Absorption Properties

Different phytoplankton groups contain diverse sets of light-absorbing pigments in addition to Chl (25, 27, 28). Light absorption is also influenced by the manner in which pigments are arranged or "packaged" within the phytoplankton (29). Absorption properties for phytoplankton can be differentiated by size class: picoplankton (<2 μm), ultraplankton (2–5 μm), nanoplankton (5–20 μm), and microplankton (>20 μm) (30). Per Chl molecule, absorption coefficients vary significantly with each size group, with picoplankton absorbing the most light and microplankton approximately eightfold less (Fig. 2*B*).

Size-specific absorption properties were input into the radiative transfer model Hydrolight (6) to investigate how phytoplankton size influences the empirical relationship. Though the general model shape was retrieved, the location of the trend line varied with each size class. Water dominated by microplankton generally had higher Chl than predicted by the ocean color algorithm (Fig. 3*A*). Conversely, water dominated by picoplankton had less Chl than that predicted by the ocean color algorithm. The average trend predicted by the OC4V4 ocean color algorithm followed the smaller size classes (picoplankton) at low Chl (0.1 mg·m^{-3}) and the larger size classes (e.g., nanoplankton) at higher Chl. This adheres to the basic concepts of biological oceanography where oligotrophic regions with low biomass tend to have small phytoplankton (e.g., *Synechococcus* and *Prochlorococcus*) (31). Larger, bloom-forming phytoplankton (e.g., diatoms and dinoflagellates) are added to the background of smaller cells in neritic waters (32). These absorption properties, although not explicit to the model formulation, are inherently built into the empirical algorithm.

Light absorption from CDOM also has considerable influence on empirical derivations of Chl, but primarily at lower Chl (<1 mg·m^{-3}), when the bluest wavelength is used in the model formulation. Surface CDOM measurements spanning the length of the Pacific Ocean ranged from 0 to 0.03 m^{-1} at 440 nm (33). Such large variability was ascribed to upwelling of deep-water masses in relationship to their age and exposure to solar degradation processes. Model results using this range of CDOM produced Chl retrievals ranging over a factor of 3 at low concentrations (<0.2 mg Chl·m^{-3}), with the OC4V4 model falling near the null CDOM at very low Chl and becoming less sensitive to CDOM at higher Chl when the formulation uses longer blue wavelengths (490 and 510 nm; Fig. 3*B*). As discussed previously, the majority of the ocean is oligotrophic, with Chl below 0.2 mg·m^{-3}, and would be particularly sensitive to spectral variability caused by CDOM (34).

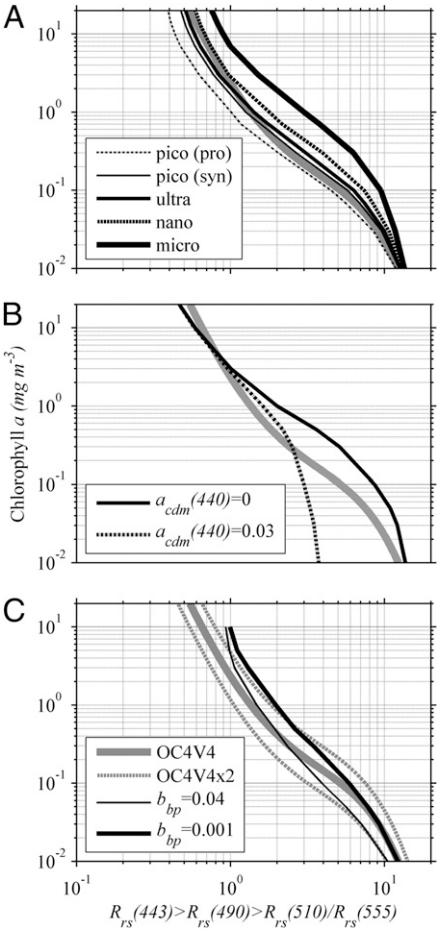

Fig. 3. Sensitivity analysis of modeled reflectance ratios vs chlorophyll for (*A*) differently sized phytoplankton modeled with fluctuating a^*_{ph} (from Fig. 2*B*); (*B*) absorption by colored dissolved matter at 440 nm (a_{cdm}) varying from 0 to 0.03 m^{-1}; and (*C*) backscattering parameterized with particulate backscattering ratios from 0.001 to 0.04. Gray dotted lines indicate values within a factor of 2 of OC4V4.

Backscattering Properties

As more phytoplankton and other particles are added to the water column, additional light is scattered out of the water (i.e., backscattered), and the spectral nature of light can be altered. Suspended sediments, like the aragonite mud on the Great Bahama Bank, highly backscatter light out of the water (35). The size, outer coating, and 3D structure all influence the specific backscattering properties of phytoplankton (36). For the world ocean, the amount of backscattered light due to suspended particles generally increases with increasing concentrations of Chl (Fig. 2*C*), and several different bio-optical models have been generated to describe this relationship (4, 37, 38). Most of these bio-optical relationships follow a power law with different slopes (Fig. 2*C*, straight lines). Many of the regional datasets, however, tend to follow a linear relationship and span a larger envelope of values. Particulate backscattering from the California coastal waters (39), for example, is significantly higher than from the Antarctic Peninsula (21). Backscattering for oligotrophic water of the North Atlantic also follows a linear relationship (40). One interpretation of these trends is that phytoplankton are added to different background levels of nonphytoplankton particles, such as sediments, minerals, detritus, and bacteria (41).

How light backscatters in water across the visible spectrums can be related to the size of the phytoplankton. Small phytoplankton, like *Synechococcus* and *Prochlorococcus*, have enhanced backscattering of blue photons. Larger phytoplankton tend to backscatter light similarly at all wavelengths, or potentially more red photons (19). To assess the sensitivity of empirical ratios to backscattering, the radiative transfer model was run with different magnitudes of spectrally invariant backscattering. Variability in backscattering alone produced twofold differences in retrieved Chl (Fig. 3*C*). In summary, changes in both the absorption and backscattering properties occur with changes in phytoplankton size structure, and both aspects have been implicitly incorporated into the present empirical approaches.

Bio-Optics of the Southern Ocean

Climate change may be most pronounced in polar regions, such as the expansive Southern Ocean (3). Recent studies have suggested that enhanced wind-driven upwelling around Antarctica caused increased ventilation of deep nutrient-rich water, linked to diatom productivity, and contributed to the deglacial rise in atmospheric CO_2 (42) Already today, winds appear to be intensifying and weakening the Southern Ocean's ability to be a sink

for CO_2 (43), and climate models project such wind intensification to persist throughout the century (44). Accurate satellite assessments of phytoplankton concentrations and, ideally, phytoplankton functional groups (i.e., diatoms associated with upwelling) in such remote locations of the ocean will be a critical component of earth's climate observing capabilities.

Bio-optical properties in different regions of the Southern Ocean lead to variability in the standard Chl retrievals. Along the Antarctic Peninsula region of the Southern Ocean, for example, ocean color algorithms were found to consistently underestimate Chl by a factor of nearly 2 for most of the Chl range (Fig. 4*A*) (45). Separate relationships have also been developed for Ross Sea waters dominated by different phytoplankton assemblages (diatoms, cryptophytes, and dinoflagellates) (46). Along the Pacific Antarctic Polar Front, a prevalence of small particles compared with Ross Sea waters produced similar overestimates of Chl using the standard algorithms (47). Coccolithophores and detached coccoliths found in the Atlantic Antarctic Polar Front elevate backscattering and may be the source of small highly scattering particles (48). In nearshore regions dominated by glacial meltwater, reflectance and backscattering can be elevated due to glacial particulates and further alter bio-optical approaches (21). These relationships were developed with the older algorithm OC2V2, which uses only reflectance at 490 nm in the numerator, but the basic trends should be similar for the wavelength-switching OC4V4. As shown, different model parameterizations can have >10-fold range in retrieved Chl.

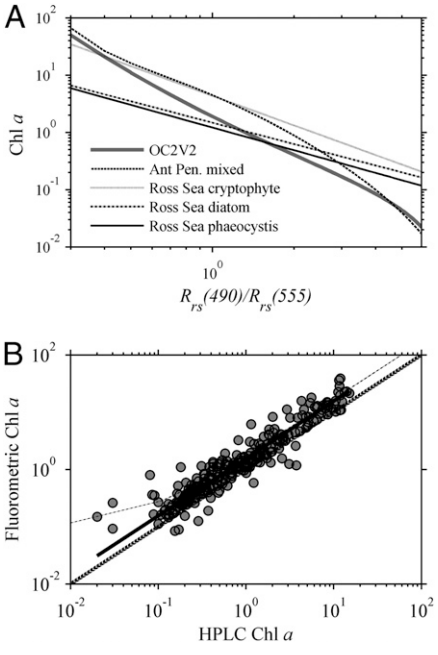

Fig. 4. (*A*) Published empirical relationships between ratios of blue-to-green reflectance, $R_{rs}(490)/R_{rs}(555)$, and chlorophyll for different regions of the Southern Ocean and phytoplankton taxa. These relationships were developed with OC2V2, but results should be similar for the wavelength-switching OC4V4 algorithm. (*B*) Data collected along the Antarctic Peninsula show fluorometrically derived Chl ≈1.7-fold higher than coincident HPLC estimates. Solid line is best fit, and light dotted line is from Antarctic Polar Front Zone (47).

Part of the apparent overestimation of Chl with empirical algorithms, for example, may be ascribed to unique pigment composition within the phytoplankton. As mentioned previously, fluorescence techniques can be erroneous as a result of varying amounts of other types of chlorophyll (*b* and *c*). Antarctic Peninsula species can have low concentrations of chlorophyll *b* and high concentrations of chlorophyll *c*, leading to higher fluorometric chlorophyll *a* than that determined with HPLC (27). Data from 2000 to 2006 collected within a few kilometers of the coast reveal a consistent offset between fluorometric and HPLC Chl (49) (Fig. 4*B*). A similar offset was observed in the Pacific sector of the Antarctic Polar Front (47), although such offsets are not ubiquitous across the Southern Ocean. The reasons for unique pigmentation in Antarctic phytoplankton are not well-defined; however, the Southern Ocean ecosystem is considered biologically unique at all trophic levels (e.g., lack of modern predators such as sharks) due to geographical barriers to invasion, physiological constraints from extreme cold temperatures, and intense seasonality of resource supplies, which make it particularly vulnerable to climate change (21). Further understanding of the spectral variability in surface waters and subsequent linkages to the trophic web will be fundamental to assessing changes in this dynamic ecosystem.

Future Directions

The relative success of Chl retrieved throughout the open ocean is remarkable given the many uncertainties in the ocean color algorithms. This achievement is generally attributed to the bio-optical assumption that ocean optical properties covary with Chl (13). Averaged over space and time, the basic biological oceanographic precepts ring true: oligotrophic regions with low biomass tend to be populated with small phytoplankton (e.g., *Synechococcus* and *Prochlorococcus*) and larger, bloom-forming phytoplankton (e.g., diatoms and dinoflagellates) predominate at higher Chl—a consequence of nutrient availability (21). Optically, this translates to high Chl-specific absorption at low Chl and low Chl-specific absorption at high Chl. These assumptions are inherently built into the empirical model, and hence Chl should not be used as an independent parameter inbio-optical models. If the standard assumptions shift due to climate change, Chl will still be derived from the empirical algorithms but with unknown accuracy.

A variety of acute and chronic hazards facing the world ocean will impact ocean biology and water color. These changes include sediment plumes, altered food webs, harmful algal blooms, changing acidity, and alterations of benthic habitats (50). Shifts in winds, clouds, and other physical forces will have profound consequences for ocean biota and ocean color. Polar regions, in particular, are exhibiting rapid changes due to shifts in climate. Along the Antarctic Peninsula, for example, the contribution of small phytoplankton has increased in the past decade, potentially due to a greater frequency of southerly winds (51). However, the Antarctic Circumpolar Current may also intensify in this region, which would promote growth of larger phytoplankton. The consequences of iron fertilization (52) and other anthropogenic activities would only serve to complicate phytoplankton dynamics further. Such complicated and potentially contradictory trends cannot be observed with simple operational empirical ratios or with approaches that delineate the optical properties within predefined ocean provinces (53).

So where do we go from here? First and foremost, ocean biology needs to be recognized as an important climate variable essential for understanding global carbon stocks and forecasting future climate. The relationships between physical forcing and biological carbon storage in the ocean are complex and not easy to predict (54). As such, accurate assessments of the quantity, production, and fate of ocean phytoplankton should be considered of high national importance and provided the necessary resources for new research and satellite missions (55). Remote sensing of ocean Chl is far from being an operational product capable of providing high-quality estimates of ocean biology under a changing climate. The current empirical algorithm assumes the ocean is a "black box" and reduces the biological, chemical, and physical diversity into simple ratios of a few spectral bands (50). As long as the ocean reflects light, the algorithm will provide a value of Chl, regardless of accuracy. Hence, caution should be applied when drawing climate-relevant conclusions from empirically derived Chl. Even in today's ocean, different conclusions have been derived from ocean color imagery to show that phytoplankton stocks have increased across the global

ocean (56) or decreased in most of the ocean basins (57).

Second, we need to move toward the use of more-analytical approaches for ocean color remote sensing. Changes in water color indicate differences in the optical properties of the surface ocean, but are not necessarily the result of varying Chl concentrations. As discussed herein, color differences can be attributed to changes in size or type of phytoplankton or to the amount of CDOM or sediments. Even changes in atmospheric gases, aerosols, or sea surface whitecaps may not be properly considered in the models. Purely statistical or empirical models are only accurate when conditions are similar to past conditions (e.g., small phytoplankton populate the oligotrophic ocean). When considering a changing ocean, the cause of the color change must be carefully assessed through semianalytical models that can separate the spectral variability due to the myriad of light absorbers and scatterers present in any water mass. Instead of simple ratios of two or more bands, these models take into account the absorption and backscattering properties of various types of phytoplankton and other compounds across the visible spectrum (58). Semianalytical models are still parameterized with some empirical components, however, and may require optimization for different regions or broad classes of water. Any such approach should be routinely validated to be accurate across a wide range of natural waters and under changing conditions. With the use of more advanced models, we can begin to ascertain the reason for changing water color and not simply attribute all spectral variability to absorption by Chl.

Third, new sensors should be launched that expand the current set of ocean color capabilities. Additional spectral channels across the visible channels will allow for better assessments of Chl and further delineation of the types of phytoplankton and their various ecological and biogeochemical roles. High-resolution spectral information between 430 and 500 nm, for example, was used to differentiate distinct absorption features of diatoms and cyanobacteria (59). More spectral information may also be useful in evaluating shallow-water benthic systems and carbon transport to the deep sea (60), and assessments of dust and aerosols for image processing. Active sensors, such as light detection and ranging (LIDAR), will allow us to probe into the depths of the oceans. In the Arctic Ocean, for example, primary production associated with the deep nutricline, not detectable with passive remote sensing, can exceed surface productivity by over an order of magnitude (9). Modeling results suggest that estimates of integrated primary productivity can be dramatically improved by incorporating the vertical distribution of phytoplankton biomass from LIDAR measurements.

Fourth, because optical constituents will not necessarily covary in the future as they do in today's ocean, comprehensive and consistent field observations must be used to assess the accuracy of satellite-derived Chl, provide better linkages to processes within the water column, and supply a regular data stream for algorithm development. Data from ships, moorings, gliders, and profiling floats (61) can provide important complementary data to satellite ocean color about the vertical structure of ocean waters as well as regions obscured by clouds. Networked systems could produce daily fields of depth-dependent optical properties not observable from space for assimilation into 3D global models. Data from sensors used to monitor aerosol variability could also prove valuable for atmospheric correction of imagery, particularly near population centers with airborne pollutants.

Furthermore, extended field observations under high solar zenith angles in concert with assimilative ocean modeling may be necessary to produce better time-averaged parameters that account for biological activity not observable by satellites. Ocean color sensors typically produce overestimates of Chl because of selective sampling in locations and times of favorable phytoplankton growth. Ocean color can only be viewed from space when clouds are not present. Although not always the case, higher Chl has been associated with periods of clear skies suitable for remote sensing (62), possibly related to a more favorable light environment for phytoplankton growth. Moreover, imagers cannot sample when sun angles are large, a common problem in high-latitude winter months. Phytoplankton populations are generally lower at these times due to light limitation, and routine undersampling from satellites at times of low biomass results in overestimates of time-averaged Chl. Such overestimations in Chl are greatest in high-latitude regions where clouds are frequent and solar zenith angles are high. Globally, this sampling bias is larger than natural interannual variability in Chl (62). Such sampling limitations should be more explicitly considered when using satellite-derived Chl for assessing global carbon stocks.

Humans cannot physically observe the vast ocean landscapes dominating Earth. In a rapidly changing world, we must rely on our "eyes in space" or satellite sensors that inform us of the status of ocean biota that help regulate atmospheric carbon. Ocean biota is not only influenced by climate change, but plays a large role in the climate cycle itself. Hence, society must move beyond operational approaches incapable of assessing a changing ocean, and invest in new and better technological approaches that can decipher the multihued ocean and the ever-changing diversity of life within.

Methods

Remote sensing reflectance, R_{rs}, represents the ratio of water-leaving radiance normalized to incident irradiance at the sea surface and is the radiometric quantity used to assess ocean color from space. The spectral quality and magnitude of R_{rs} is governed by the water's optical properties and is proportional to the ratio of light scattered in the backward direction out of the water column (i.e., backscattering, b_b) to absorption (a), such that (4)

$$R_{rs} \propto \frac{b_b}{a + b_b}$$

A radiative transfer model, Hydrolight, was used to estimate R_{rs} with various environmental input parameters (6). The model was run with four different optically active components corresponding to pure water (15), phytoplankton, CDOM, and minerals (set to null). To assess variability of R_{rs} with different absorptive properties, the Chl-specific phytoplankton absorption, $a^*_{ph}(\lambda)$, for each size class was input into the model (30). Chl was assumed to be constant with depth and ranged from 0.01 to 60 mg·m^{-3}. For the first sensitivity analysis, absorption by CDOM was proportional to Chl absorption at a reference wavelength following an exponential relationship (F = 1, λ_0 = 440; γ = 0.014) (6). Inelastic scatter from Chl, CDOM, and Raman scattering were included. A semiempirical clear sky model with a solar zenith angle of 55° was used with 5 m·s^{-1} winds. Scattering was modeled with a Chl-specific power-law dependence on wavelength with near-surface coefficients (b_0 = 0.407; λ_0 = 660, n = 0.75, and m = 1) (37). The particle-phase function, which determines the fraction of light that is backscattered, was modeled from Fournier-Forand (FF) with different amounts of backscatter fraction (b_b/b) varying with Chl (39). For the CDOM sensitivity analysis, the model was run with $a^*_{ph}(\lambda)$ for ultraplankton and with varying CDOM levels from 0 to 0.03 m^{-1}. For the backscattering sensitivity analysis, the backscattering fraction was modeled as either 0.04 or 0.001 for all levels of Chl, and phytoplankton absorption properties were allowed to vary bio-optically with Chl (29).

ACKNOWLEDGMENTS. Many individuals have contributed to my thoughts and research on this topic, including Aurea Ciotti, Michael Twardowski, James Sullivan, and Richard Zimmerman. Thanks to SeaWiFS Project Office for imagery. Financial support was provided by the National Aeronautics and Space Administration (NASA) Ocean Biology and Biogeochemistry Group, and the Environmental Optics Division, Office of Naval Research.

1. Longhurst A, Sathyendranath S, Platt T, Caverhill C (1995) An estimate of global primary productivity in the ocean from satellite radiometer data. *J Plankton Res* 17:1245–1271.

2. Behrenfeld MJ, et al. (2006) Climate-driven trends in contemporary ocean productivity. *Nature* 444:752–755.

3. Joseph J (1950) Investigations of above and underwater light measurements in the sea and connection with transparency measurements (Translated from German). *Dtsch Hydrographische Z* 3:324–335.
4. Gordon HR, Morel AY (1983) *Remote Assessment of Ocean Color for Interpretation of Satellite Visible Imagery: A Review* (Springer, New York).
5. Zaneveld JRV (1973) *Optical Aspects of Oceanography*, ed Jerlov NG (Academic, San Diego), pp 121–134.
6. Mobley CD (1994) *Light and Water: Radiative Transfer in Natural Waters* (Academic, San Diego).
7. Polovina JJ, Howell EA, Abecassis M (2008) Ocean's least productive waters are expanding. *Geophys Res Lett* 35:1–5.
8. Irwin AJ, Oliver MJ (2009) Are ocean deserts getting larger? *Geophys Res Lett*, 10.1029/2009GL039883.
9. Hill V, Cota G (2005) Spatial patterns of primary production on the shelf, slope and basin of the Western Arctic in 2002. *Deep Sea Res Part II Top Stud Oceanogr* 52:3344–3354.
10. Falkowski P, et al. (2000) The global carbon cycle: A test of our knowledge of earth as a system. *Science* 290:291–296.
11. Carr ME, et al. (2006) A comparison of global estimates of marine primary production from ocean color. *Deep Sea Res Part II Top Stud Oceanogr* 53:741–770.
12. Platt T, Bouman H, Devred E, Fuentes-Yaco C, Sathyendranath S (2005) Physical forcing and phytoplankton distributions. *Scientia Marina*, 10.3989/scimart.2005.69s155.
13. IPCC W (2007) *Contribution of Working Group I to the Fourth Assessment Report of the Intergovernmental Panel on Climate Change*, eds Solomon S, et al. (Cambridge Univ Press, Cambridge, UK).
14. IOCCG (2008) Why Ocean Colour? The Societal Benefits of Ocean Colour Technology, eds Platt T, et al. Reports of the International Ocean-Colour Coordinating Group, No. 7 (IOCCG , Dartmouth, NS, Canada), pp 83–102.
15. O'Reilly JE, et al. (2000) SeaWiFS Postlaunch Calibration and Validation Analyses, Part 3. *NASA Tech. Memo. 2000-206892*, eds Hooker SB, Firestone ER, (NASA Goddard Space Flight Center), Vol 11, 49 pp.
16. McClain CR (2009) A decade of satellite ocean color observations*. *Annu Rev Mar Sci* 1:19–42.
17. O'Reilly JE, Maritorena S, Mitchell BG, Siegel DA (1998) Ocean color chlorophyll algorithms for SeaWiFS. *J Geophys Res* 103:24937–24953.
18. Schofield O, et al. (2004) Watercolors in the coastal zone: What can we see? *Oceanography* 17:24–31.
19. Dierssen HM, Kudela RM, Ryan JP, Zimmerman RC (2006) Red and black tides: Quantitative analysis of water-leaving radiance and perceived color for phytoplankton, colored dissolved organic matter, and suspended sediments. *Limnol Oceanogr* 51:2646–2659.
20. Moline MA, Claustre H, Frazer TK, Schofield O, Vernet M (2004) Alteration of the food web along the Antarctic Peninsula in response to a regional warming trend. *Global Change Biol*, 10:1973–1980; 10.1111/j.1365-2486.2004.00825.x.
21. Dierssen HM, Smith RC, Vernet M (2002) Glacial meltwater dynamics in coastal waters west of the Antarctic peninsula. *Proc Natl Acad Sci USA* 99:1790–1795.
22. Hooker SB, Lazin G, Zibordi G, McLean S (2002) An evaluation of above- and in-water methods for determining water-leaving radiances. *J Atmos Oceanic Technol* 19:486–515.
23. Mueller JL, et al. (2003) Ocean optics protocols for satellite ocean color sensor validation, revision 5, volume V: Biogeochemical and bio-optical measurements and data analysis protocols. NASA Tech. Memo 211621 (NASA Goddard Space Flight Center, Greenbelt, MD).
24. Trees CC, Kennicutt MC, Brooks MJ (1985) Errors associated with the standard fluorometric determination of chlorophylls and phaeopigments. *Mar Chem* 17:1–12.
25. Kumari B (2005) Comparison of high performance liquid chromatography and fluorometric ocean colour pigments. *J Ind Soc Remote Sensing* 33:541–546.
26. Marrari M, Hu C, Daly K (2006) Validation of SeaWiFS chlorophyll *a* concentrations in the Southern Ocean: A revisit. *Remote Sens Environ* 105:367–375.
27. Sathyendranath S, Lazzara L, Prieur L (1987) Variations in the spectral values of specific absorption of phytoplankton. *Limnol Oceanogr* 32:403–415.
28. Claustre H, et al. (2004) An intercomparison of HPLC phytoplankton pigment methods using in situ samples: Application to remote sensing and database activities. *Mar Chem* 85:41–61.
29. Bricaud A, Babin M, Morel A, Claustre H (1995) Variability in the chlorophyll-specific absorption coefficients of natural phytoplankton: Analysis and parameterization. *J Geophys Res* 100:13321–13332.
30. Ciotti AM, Cullen JJ, Lewis MR (2002) Assessment of the relationships between dominant cell size in natural phytoplankton communities and the spectral shape of the absorption coefficient. *Limnol Oceanogr* 47:404–417.
31. Olson RJ, Chisholm SW, Zettler ER, Armbrust EV (1990) Pigments, size, and distribution of *Synechococcus* in the North Atlantic and Pacific Oceans. *Limnol Oceanogr* 35:45–58.
32. Yentsch CS, Phinney DA (1989) A bridge between ocean optics and microbial ecology. *Limnol Oceanogr* 34:1694–1705.
33. Swan CM, Siegel DA, Nelson NB, Carlson CA, Nasir E (2009) Biogeochemical and hydrographic controls on chromophoric dissolved organic matter distribution in the Pacific Ocean. *Deep Sea Res Part I Oceanogr Res Pap* 56:2175–2192.
34. Morel A, Gentili B, Chami M, Ras J (2006) Bio-optical properties of high chlorophyll case 1 waters and of yellow-substance-dominated case 2 waters. *Deep Sea Res Part I Oceanogr Res Pap* 53:1439–1459.
35. Dierssen HM, Zimmerman RC, Burdige DJ (2009) Optics and remote sensing of Bahamian carbonate sediment whitings and potential relationship to wind-driven Langmuir circulation. *Biogeosciences* 6:487–500.
36. Stramski D, Boss E, Bogucki D, Voss KJ (2004) The role of seawater constituents in light backscattering in the ocean. *Prog Oceanogr* 61:27–56.
37. Loisel H, Morel A (1998) Light scattering and chlorophyll concentration in case 1 waters: A reexamination. *Limnol Oceanogr* 43:847–858.
38. Huot Y, Morel A, Twardowski MS, Stramski D, Reynolds RA (2008) Particle optical backscattering along a chlorophyll gradient in the upper layer of the eastern South Pacific Ocean. *Biogeosciences* 5:495–507.
39. Sullivan JM, Twardowski MS, Donaghay PL, Freeman SA (2005) Use of optical scattering to discriminate particle types in coastal waters. *Appl Opt* 44:1667–1680.
40. Siegel DA, Maritorena S, Nelson NB, Behrenfeld MJ (2005) Independence and interdependencies among global ocean color properties: Reassessing the bio-optical assumption. *J Geophys Res*, 10.1029/2004JC002527.
41. Behrenfeld MJ, Boss E, Siegel DA, Shea DM (2005) Carbon-based ocean productivity and phytoplankton physiology from space. *Global Biogeochem Cycles*, 10.1029/2004GB002299.
42. Anderson RF, et al. (2009) Wind-driven upwelling in the Southern Ocean and the deglacial rise in atmospheric CO2. *Science* 323:1443–1448.
43. Le Quéré C, et al. (2007) Saturation of the southern ocean CO2 sink due to recent climate change. *Science* 316:1735–1738.
44. Kohfeld KE, Le Quéré C, Harrison SP, Anderson RF (2005) Role of marine biology in glacial-interglacial CO2 cycles. *Science* 308:74–78.
45. Dierssen H, Smith RC (2000) Bio-optical properties and remote sensing ocean color algorithms for Antarctic Peninsula waters. *J Geophys Res* 105:26301–26312.
46. Arrigo KR, Robinson DH, Worthen DL, Schieber B, Lizotte MP (1998) Bio-optical properties of the southwestern Ross Sea. *J Geophys Res* 193:21683–21695.
47. Reynolds RA, Stramski D, Mitchell BG (2001) A chlorophyll-dependent semianalytical reflectance model derived from field measurements of absorption and backscattering coefficients within the Southern Ocean. *J Geophys Res* 106:7125–7138.
48. Balch WM, Gordon HR, Bowler BC, Drapeau DT, Booth ES (2005) Calcium carbonate measurements in the surface global ocean based on Moderate-Resolution Imaging Spectroradiometer data. *J Geophys Res*,10.1029/2004JC002560.
49. Kozlowski W (2008) Pigment derived phytoplankton composition along the western Antarctic Peninsula. Master's thesis (San Diego State Univ, San Diego).
50. Zanevelt JR (2006) Reports of the International Ocean-Colour Coordinating Group, No. 5. *Remote Sensing of Inherent Optical Properties: Fundamentals, Tests of Algorithms, and Applications*, ed Lee ZP (IOCGG, Dartmouth, NS, Canada), pp 3–12.
51. Montes-Hugo MA, Vernet M, Martinson D, Smith R, Iannuzzi R (2008) Variability on phytoplankton size structure in the western Antarctic Peninsula (1997–2006). *Deep Sea Res Part II Top Stud Oceanogr* 55:2106–2117.
52. Chisholm S, Falkowski P, Cullen J (2001) Oceans. Discrediting ocean fertilization. Science's Compass. *Science* 294:309–310.
53. Longhurst AR (2007) *Ecological Geography of the Sea* (Academic, San Diego).
54. Marinov I, et al. (2008) Impact of oceanic circulation on biological carbon storage in the ocean and atmospheric pCO2. *Global Biogeochem Cycles*, 10.1029/2007GB002958.
55. Seibel BA, Dierssen HM (2009) Ocean science. Animal function at the heart (and gut) of oceanography. *Science* 323:343–344.
56. Antoine D, Morel A, Gordon HR, Banzon VF, Evans RH (2005) Bridging ocean color observations of the 1980s and 2000s in search of long-term trends. *J Geophys Res*, 10.1029/2004JC002620.
57. Gregg WW, Casey NW, McClain CR (2005) Recent trends in global ocean chlorophyll. *Geophys Res Lett*, 10.1029/2004GL021808.
58. Lee ZP, ed (2006) *Remote Sensing of Inherent Optical Properties: Fundamentals Tests of Algorithms, and Application*. Reports of the International Ocean-Colour Coordinating Group, No. 5 (IOCCG, Dartmouth, NS, Canada).
59. Bracher A, et al. (2009) Quantitative observation of cyanobacteria and diatoms from space using PhytoDOAS on SCIAMACHY data. *Biogeosciences* 6:751–764.
60. Dierssen HM, Zimmerman RC, Drake LA, Burdige DJ (2009) Potential export of unattached benthic macroalgae to the deep sea through wind-driven Langmuir circulation. *Geophys Res Lett*, 10.1029/2008GL036188.
61. Boss E, et al. (2008) Observations of pigment and particle distributions in the western North Atlantic from an autonomous float and ocean color satellite. *Limnol Oceanogr* 53:2112–2122.
62. Gregg WW, Casey NW (2007) Sampling biases in MODIS and SeaWiFS ocean chlorophyll data. *Remote Sens Environ* 111:25–35.